6th International Meeting
on
Wind Turbine Noise
Glasgow 20-23 April 2015

Impact on Flow Topology of Solid and Permeable Trailing Edge Serrations at Incidence on Cambered and Symmetric Airfoils

Carlos Arce, Delft University of Technology, the Netherlands, and LM Wind Power, Denmark, E-mail: c.a.arceleon-2@tudelft.nl

Daniele Ragni, Delft University of Technology, the Netherlands, E-mail: d.ragni@tudelft.nl

Stefan Pröbsting, Delft University of Technology, the Netherlands, E-mail: s.probsting@tudelft.nl

Jesper Madsen, LM Wind Power, Denmark, E-mail: jema@lmwindpower.com

Summary

Test solid and permeable trailing edge serration designs are applied to a NACA 0018 and a DU96-W-180 airfoil. They are set at incidence through changes in flap angle and airfoil angle of attack, and the flow is characterized using stereoscopic particle image velocimetry (PIV) and complimented numerically using Reynolds-averaged Navier-Stokes equations (RANS). Time averaged flow velocity components and turbulence statistics are extracted, from which flow sensitivity is found to be higher for flap angle induced incidence when compared to incidence prescribed through changes in angle of attack. The benefits of permeable serration designs are furthermore highlighted, accentuated by the notable reduction of flow blockage effects when compared to solid serrations in time averaged and turbulence observations which, if avoided, could allow the use of serrations under a wider operation envelope, keeping the benefits of a serrated trailing edge without heavily disturbing the turbulence and flow characteristics which, if done, could instead result in the generation of additional noise sources.

1. Introduction

The problem of wind turbine noise is a complex and multidisciplinary one that encompasses a comprehensive range of topics in the already wide subject of acoustics. None withstanding, as a consequence of the current trend of increasing rotor size and the benefits of using designs that promote faster tip speed ratios, the noise from wind turbines is today more commonly dominated by aeroacoustic borne sources, notably influenced by emissions from the outboard sections of the rotating blades (Oerlemans, Sijtsma, and López, 2007).

The propagation of acoustic waves in the atmosphere, and the mechanisms involved in the phenomenon of amplitude modulation, are in themselves subjects of great depth, yet at their core, understanding the problem of wind turbine noise starts at what happens to the flow close to the blade and its interaction with the blade surface, having the target of identifying the physics responsible for causing the dominant noise. It is argued that during the normal operation of a state-of-the-art horizontal axis wind turbine blade, the prevalent source of airfoil self-noise is turbulent boundary layer trailing edge noise (Brooks, Pope, and Marcolini, 1989).

Aside from having been shown useful in mitigating noise from other types of airfoil noise mechanisms, such as laminar vortex shedding noise (Chong, Joseph, and Gruber, 2012), the application of devices at the trailing edge have shown promise in mitigating noise from the turbulent boundary layer flow interaction with the trailing edge and its scattering mechanisms. One increasingly common approach to such a device is the serrated trailing edge, of which a simple embodiment consists of a flat plate attachment or insert that has the appearance of triangles protruding from the trailing edge of an airfoil or blade section. Serrations are explained to be efficient noise reduction devices by having a twofold effect. The change from straight to a serrated beneficially affects the acoustic scattering properties of the sharp trailing by changing the spanwise length of the trailing edge that contributes to noise generation (Howe, 1991). Additionally, the presence of the serration as a solid surface is argued to drive changes in the flow structure and turbulence properties that disturb its efficiency to contribute to noise emission (Moreau, 2012; Gruber, Azarpeyvand, and Joseph, 2010). Nevertheless, larger changes in flow topology could instead degrade the design performance targets of the airfoil, and potentially turn the serrations into an additional source of noise themselves.

Motivated by these principles, and inclined towards finding a solution to the problem of designing trailing edge serrations for full scale wind turbine blade applications, the work herein presented focuses on the effect that serration incidence has on the flow. It also focuses on novel serration designs that intend to reduce the potentially unwanted effects that incidence might have on the flow, for which purpose a 50% permeable serration was constructed, inspired by one previously studied in Gruber, Joseph, and Azarpeyvand, 2013.

This slitted design is shown there to have an improved performance in noise reduction when compared to the traditional solid serrations, which instead exhibited an increase of noise emission at higher frequencies against the unserrated baseline airfoil case. This unwanted effect is argued to be a consequence of the serrations not being aligned with the flow, and has also been reported in Dassen et al., 1996; Moreau, Brooks, and Doolan, 2011; Oerlemans et al., 2009.

The flow is experimentally investigated using particle image velocimetry (PIV), and numerically using Reynolds averaged Navier-Stokes equations (RANS). Using these methods, the flow sensitivity to different degrees of incidence is established, along with differences found in turbulence statistics. The analysis aims at characterizing the effect that incidence and serration porosity have on the flow, with a suggested extension towards how the noise mitigation performance of serrations could be affected.

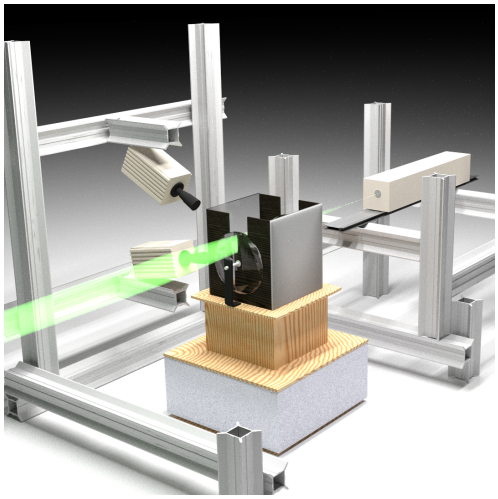

(a) Rendered overview of the NACA 0018 campaign setup

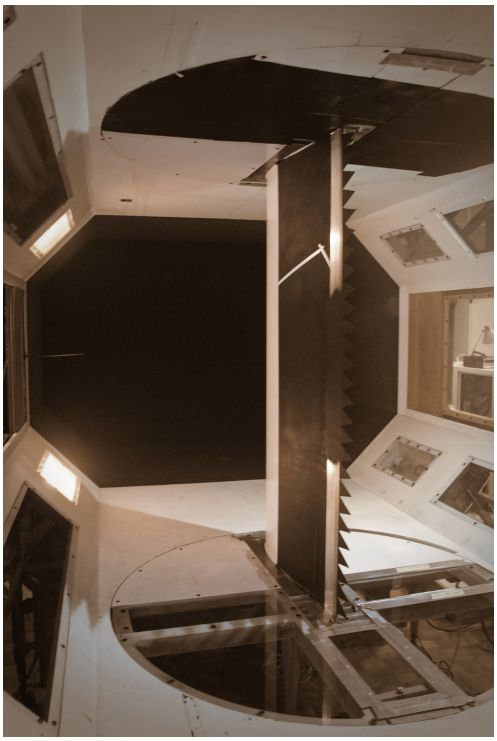

(b) Photograph of the serrated DU96 airfoil mounted inside TU Delft's LTT wind tunnel

Figure 1: Overview of the two campaign setups.

2. Experimental setup

Two experimental campaigns were conducted in order to establish the relation of serration incidence and porosity on flow topology on two distinct airfoil models, one symmetric and one with camber.

2.1. NACA 0018 campaign

The first campaign was performed using a NACA 0018 airfoil, chosen based on that similar airfoil thicknesses are used at the outboard sections of large commercial blade designs. The fact that it is symmetric makes it differ from commonly used blade airfoil sections, but simplifies the task of defining the baseline case, namely that for which the serrations are set at a neutral position and not at incidence, or rather, when there is not a significant pressure difference between their upper and lower sides.

These measurements were conducted at the open jet vertical wind tunnel facility of the Technological University of Delft (TU Delft). This wind tunnel has a contraction ratio in the order of 60:1, terminating in a nozzle of 40 cm by 40 cm, resulting in flow having low turbulence intensity, while reaching speeds of up to around 50 m/s. The airfoil spans the width of the wind tunnel nozzle exit and is enclosed in a test section of four sides, one of which is constructed out of transparent Plexiglas to allow capturing the images needed for the PIV campaign. The chord of the airfoil is $C = 20$ cm. A rendering of the setup can be seen in figure 1a, where the vertical wind tunnel nozzle and test section can be seen, along with the laser on the right and the location of the two cameras looking through the test section.

The boundary layer was made turbulent by tripping with a carborundum strip of 1 cm thickness at a location of $0.175x/C$. Considering the chord length and the relative size of the tripping strip, this method was preferred over the use of zigzag tape in order to avoid the risk of creating periodic flow patterns that could convect down past the trailing edge, increasing the potential of contaminating the patterns in the flow caused by the serrations.

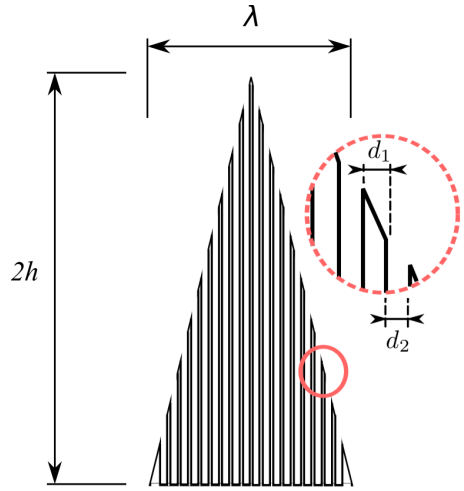

Figure 2: Slitted permeable serration design

The tested parameters consisted of permutations between three different flow speeds, 10, 20, and 40 m/s, three angles of attack, $\alpha = 0°$, $3°$, and $6°$, and three serration flap angles, $\varphi = 0°$, $3°$, and $6°$. The flap angles follow traditional flap angle nomenclature, where positive indicates a rotation towards the lower airfoil side. The prescribed flow speeds result in measurements run at Reynolds numbers of around 130 000, 260 000 and 520 000. The serrations themselves were of a flat plate design, with a thickness of 1 mm, and an amplitude of $2h = 0.2C$. A serration wavelength of $\lambda = h$ was used. The serrations were constructed in two different designs: one solid and one 50% permeable. The latter was made by cutting slits in a streamwise direction, with the slits having equal width as the space between them, namely $d_1 = d_2 = 0.0025C$, and spanning the entirety of the local serration length (see figure 2). The design of the airfoil and the serrations was such that it allowed for the serration panel to be inset at the trailing edge, resulting in a smooth transition.

The PIV system used was a high speed setup using a dual cavity Nd:YLF laser for illumination, and the images were captured using two Photon Fastcam SA1 with a CMOS sensor able to capture a resolution of 1024×1024 pixels. The setup was controlled by a LaVision high speed controller operated with DaVis 8.1 software. The cameras were equipped with Nikkor objectives of 105 mm and 180 mm focal length, providing a suitable field of view for each of the the two different fields of view captured in this campaign, corresponding to one in close proximity to the surface of the serrations, approximately at about 1 mm $\sim 0.1\delta$, on both the pressure and suction side. And the other plane was located 1.5 serration amplitudes downstream, perpendicular to the free stream.

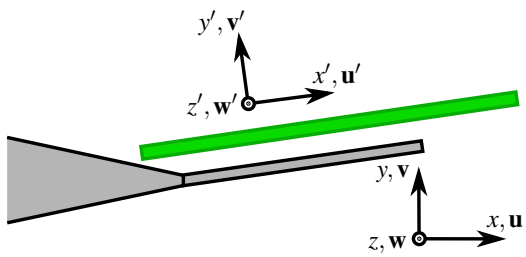

Figure 3: Definition of the coordinate systems used for the result discussion.

Since the measurement plane close to the surface is slanted in respect to the general coordinate system, the system (x', y', z') is used instead to describe these measurements, as shown in figure 3, where the measurement plane is represented by the green line, indicating the location of the laser sheet over the serration surface in a non-zero flap angle case.

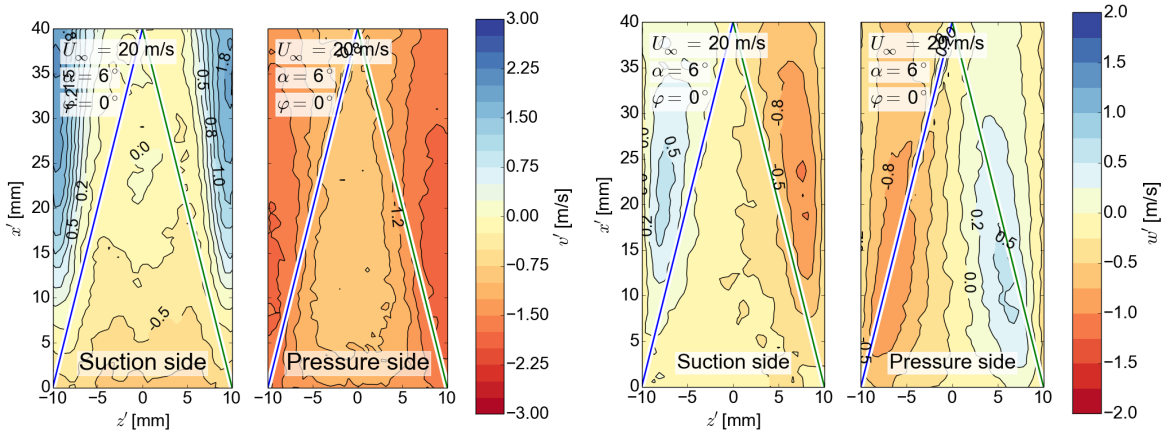

(a) v' component (b) w' component

Figure 4: Suction and pressure side flow components for the solid serrations.

3. Experimental results

A discussion on the experimental results is presented below, starting with a discussion on the measured time average flow velocity components for the solid serration near the surface, followed by the near surface measurements of the porous serrations, and the cross flow measurement comparisons for both. Lastly an analysis of turbulence related statistics is presented.

3.1. Effect of incidence of a solid serration on near surface flow topology, NACA 0018

As could be expected, when the solid serrations are set at incidence, the flow close to the pressure side surface was seen in the experiment to suffer a deviation from the free stream direction and being forced to a certain degree to find way through the space between adjacent serrations. Observing figure 4b, this effect can be seen in the increased magnitude of the lateral velocity component of the flow, w', on the pressure side close to the trailing edges of the serration, when compared to regions closer to the serration midline. Here the serration trailing edge is outlined and the measurement plane is located 2 mm over and parallel to its surface.

The out of plane v' component plot in figure 4a further suggests that the flow suffers a strong acceleration in the regions between serrations, showing it as it seeps through this space, being forced to flow around the serration. This strong vertical component is replicated both in the suction and pressure sides and creates a region that significantly influences the behavior of the flow close to the serration suction side surface which, as it convects past the trailing edge, becomes affected by the pressure side flow.

This side effect is evidenced suction side the w' component plot of figure 4b, which shows a marked difference in behavior when compared to the above discussed v' component measured for the flow close to the pressure side surface. Contrary to the latter, the suction side flow sees bending in the direction of the serration middle line and becomes somewhat aligned to the serration trailing edge, especially in regions around the serration half length. Moreover, it remains practically unaffected while it convects over most of the serration surface.

Serration incidence showed a different degree of influence on the flow, depending on which

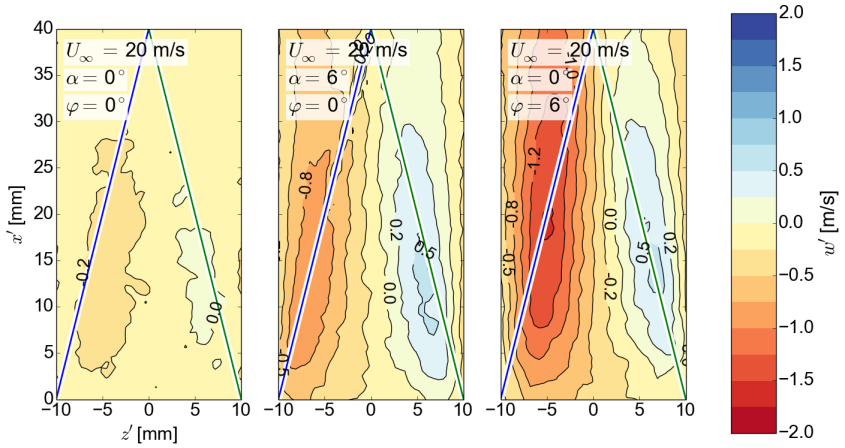

Figure 5: Comparison of incidence parameter effect on spanwise flow deflection.

parameter is prescribed to induce it, namely angle of attack or serration flap angle. Figure 5 exemplifies this by comparing the effect on w' of incidence purely prescribed through a change in angle of attack, and one where it is only due to flap angle, showing the latter to have a more significant effect on the flow. A detailed discussion of this is presented in Arce et al., 2015, and it is argued that the cause of this variation lies in that a change in angle of attack will likely create a wider effect on the flow around the airfoil and its wake. The serration flap angle is instead of a more local nature, creating a sharper geometric discontinuity that affects the flow more suddenly. Further measurements showed that variations in mean flow velocity were not found to create a notable difference in flow behavior.

3.2. Effect of incidence of a porous serration on near surface flow topology, NACA 0018

The difference in noise mitigation performance seen in Gruber, Joseph, and Azarpeyvand, 2013 by the slitted porous serration compared to the solid serration design suggests that differences in flow behavior happening close to its surface and in the wake are plausible.

Indeed, when looking at the flow v' component as plotted in figure 6a, it is seen to have magnitudes and direction that effectively suggest the existence of flow transfer through the porous surface. In addition it is markedly different from the solid case seen above, showing velocity gradients across the z axis that are shallower in comparison, and the presence of the higher speed regions in the space between serration teeth is largely gone.

A gradient is also seen in the x' direction on both the pressure and suction sides, and which is not shared by the pressure side result of the solid serration. The negative sign suggests that the flow in the slitted case finds a broader freedom to flow vertically towards the serration surface, while the solid serration case shows values much closer to zero, indicating almost null vertical movement of the flow.

Likewise, in the suction side result for the slitted serration, higher out of plane values are evident, while the solid case exhibits only values that are closer to zero. Again, this suggests that flow experiences a certain amount of freedom to flow through the serration porous surface.

The w' component result of figure 6b further indicates that the porosity in the slitted serrations

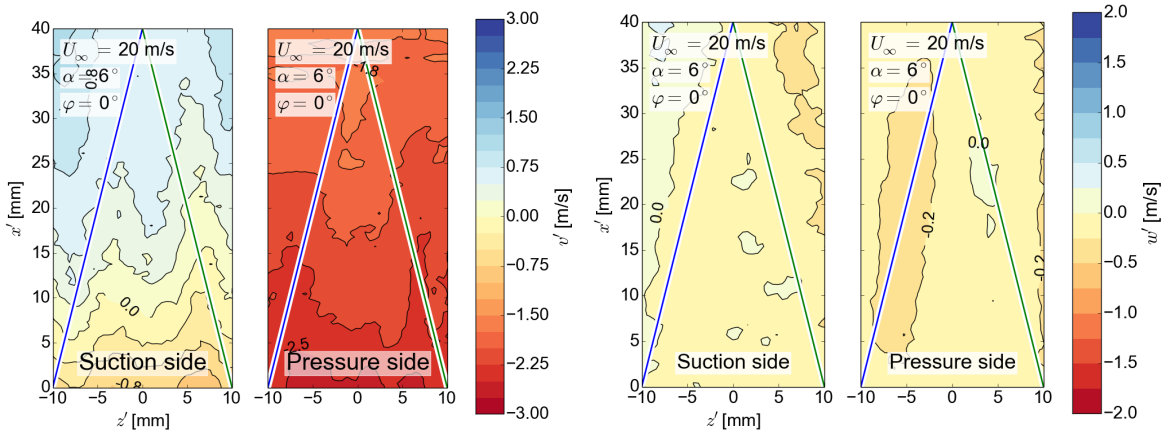

(a) v' component (b) w' component

Figure 6: Suction and pressure side flow components for the slitted serrations.

helps to avoid the amount of blockage induced by the serration incidence, allowing to mitigate the flow digression seen in figure 4b for the solid serrations.

The fact that noticeable differences were seen in flow behavior between the slitted serration design versus the solid design under the same conditions, added to the fact that they have previously been measured acoustically to perform better than the latter, shows promise in the understanding of what kind of flow properties one might be interested in achieving when aerodynamically designing trailing edge devices, while confirming that the serrated shape of the modified trailing edge has appeared indeed to be effective for noise mitigation. This knowledge can hopefully be used to further the advancements in trailing edge device designs for noise mitigation, especially when one considers particular conditions and applications.

3.3. Cross flow measurements

The effect of serrations is also visible in the wake region, most clearly in the formation of streamwise vortices that shed from the left and right trailing edges of the serration. A contour plot of streamwise vorticity can be seen in figure 7a for selected cases of the NACA 0018 campaign. For all these visualizations, a serration tip is roughly located at the axis origin and the axes are in units of serration wavelength, λ.

The effect of serration flap angle is evident for the solid serration design, where, for an angle of attack of $\alpha = 6°$, a flap angle of $\varphi = 0°$ exhibits the formation of two streamwise vortices, shedding from the left and right trailing edges of the serration respectively in a clock and anti-clockwise direction. Deflecting the serration by $\varphi = 6°$ has the effect of roughly triplicating the rotational frequency of these vortices.

The performance of the slitted serration design is also evident in these results, like it was for the near surface measurements. When comparing with the analogue case for the solid serrations, they seem to play instead no part in the formation of streamwise vortical structures.

The presence of streamwise vortices is also evident in the DU96 campaign measurements, figure 7b. The effect of angle of attack is seen in their intensity, while the baseline case shows a

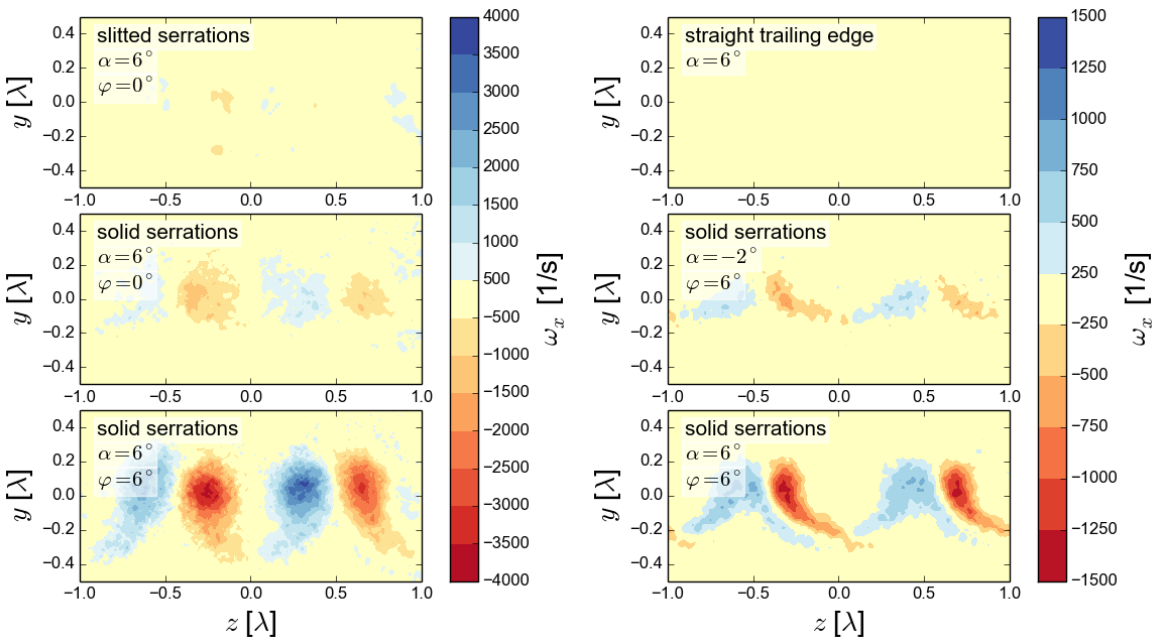

(a) NACA 0018, $1.5 \times 2h$ downstream of the serrations

(b) DU96, $0.5 \times 2h$ downstream of the serrations

Figure 7: Spanwise vorticity as measured in the wake.

clean field with no vortical structures present, as would be expected. The behavior is similar to that of the NACA 0018 campaign, nevertheless the structures appear more elongated and with smaller cores. This effect is likely due to the closer location of the measurements to the serration tips compared to the NACA 0018 case; h versus $3h$. The overall intensity is also decreased in the DU96 campaign by around half of that found in the NACA 0018 measurements.

3.4. Turbulence analysis

In order to establish changes in the flow turbulence properties, a quadrant and a spanwise cross-correlation analysis has been performed on the data. No turbulence spectra are drawn from the measured data as the acquisition rate is kept low to perform the time averaged results presented above, allowing to achieve good convergence in the averaged statistics in lieu of loss of time resolution. In total, 1500 samples are obtained for each case, with a frequency in the order of 1×10^2 Hz. It must be therefore stressed that this analysis does not presume as of yet to suggest a link between the observed turbulence trends with the aeroacoustic noise differences of the two serration designs observed in Gruber, Joseph, and Azarpeyvand, 2013.

For a Reynolds decomposition of the flow, such that $U(\vec{x},t) = \bar{U}(\vec{x}) + \dot{U}(\vec{x},t)$ where $\bar{U}(\vec{x})$ is the time averaged result of U and $\dot{U}(t)$ is its time dependent perturbations, a quadrant analysis shows the relationship of the plane normal component, $\dot{v}'(\vec{x}',t)$ and the free stream parallel component, $\dot{u}'(\vec{x}',t)$ as a scatter plot. The resulting shape of the scatter cloud is an interpretation of the turbulence properties and flow structures at a particular point in space. The location of the individual measurements indicate if at that given moment that region saw an ejection, sweep, outward, or inward event depending on which quadrant the $(\dot{u},\dot{v})$ result falls

into. See figure 8, and Willmarth and Lu, 2006 for a detailed explanation.

The quadrant analysis is performed over 42 points over the serration surface, 7 in the z' direction and 6 in the x' direction. The location of the points is seen in figure 9, where the outline of the serration is drawn for clarity. All measurement point coordinates are given in millimeters.

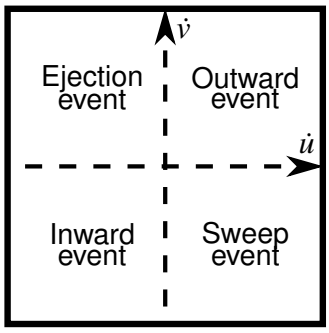

Figure 8: Quadrant analysis

There are clear differences between the quadrant analysis plots of the three presented cases and among locations for each individual case. The solid serration presents, figure 10a, rather scattered samples, accentuated on locations over the serration surface and with a slightly higher concentration at regions above empty space. The classic oval shape indicating ejection and sweep events in a boundary layer is evident and more defined in the regions closer to the airfoil trailing edge. As the flow moves downstream it loses the oval definition slightly, but where this difference is most noticeable is again in the empty regions between adjacent serrations.

The slitted serrations, figure 10b, show a distinctly different behavior that approximates the trends in the straight trailing edge (figure 10c) more closely than the solid serration quadrant patterns. Close to the airfoil trailing edge, the scatter pattern is similar between the slitted and solid serrations, but for the former it becomes concentrated and circular in shape more rapidly for points downstream. It could be argued that the shape of the serration can be visually identified in the quadrant patterns, but if so it's only due to slight variations between them, the effect being more noticeable by moving downstream rather than laterally.

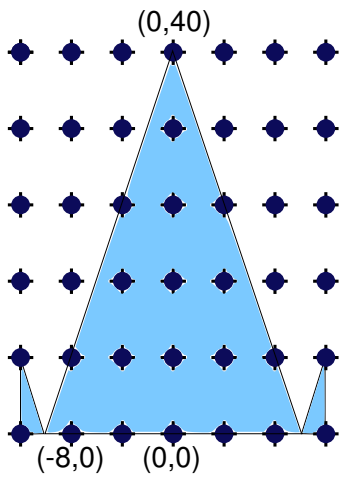

Figure 9: Quadrant analysis point locations.

Differences between the slitted serration and straight trailing edge amount mostly to the behavior close to the airfoil trailing edge, where the former case presents a behavior similar to the solid serrations where an ejection-sweep behavior is noticeable in the flow, while the latter shows scattering mostly dominated by the v' component, with less variation over the u' component, and no apparent correlation between the two.

The component-wise turbulence cross-correlation is calculated as

$$r(\Delta\vec{x}) = \frac{\sum_{i=1}^{n} \dot{u}(\vec{x}_0)_i \, \dot{u}(\vec{x})_i}{\sqrt{\sum_{i=1}^{n} \dot{u}(\vec{x}_0)_i \sum_{i=1}^{n} \dot{u}(\vec{x})_i}}$$

for $\dot{u}$ any time variant perturbation time series component of the flow velocity vector $\vec{U}$ separated by a spatial distance $\Delta\vec{x} = \vec{x} - \vec{x}_0$, for which, to get spanwise cross-correlation, $\vec{x} = (0, 0, z')$ and $\vec{x}_0 = (x', y'_0, z'_0)$.

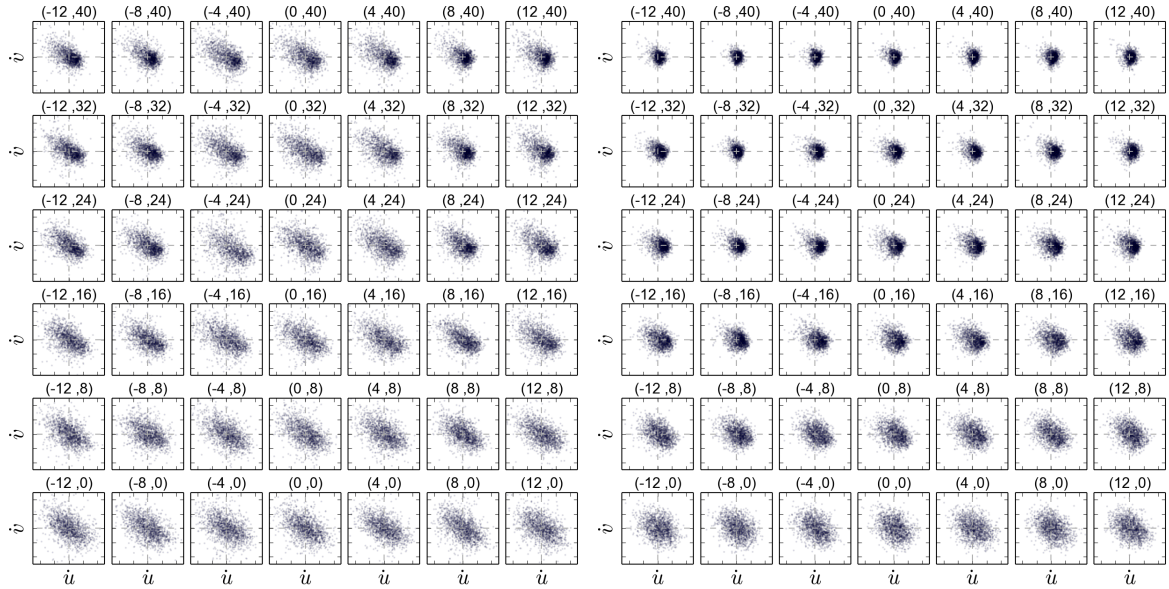

(a) Solid serration

(b) Slitted serration

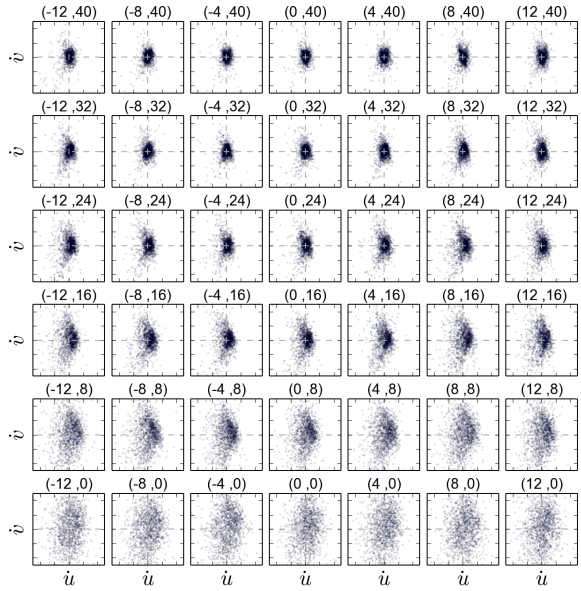

(c) Straight trailing edge

Figure 10: Quadrant analysis for $\alpha = 6°$, $\varphi = 0°$, and $U_\infty = 20$ m/s, pressure side.

In figure 11, the values of the spanwise cross-correlation coefficient can be seen for $z_0' = 0$. The setup is the same as discussed before for the quadrant analysis, where $\alpha = 6°$, $\varphi = 0°$, and $U_\infty = 20$ m/s. Maximum cross-correlation is naturally achieved close to the center line of the serration, $z_0' = 0$ mm, nevertheless differences between the three cases shown are already noticeable close to z_0'. While the slitted serrations and the straight trailing edge behave similar, the solid serrations show higher cross-correlation over a larger spanwise distance.

As the flow moves downstream, the straight trailing edge case shows an increased cross-correlation seen starting slightly after 20 mm and more significantly after 30 mm, perhaps due to the turbulence gaining homogeneity at this location in the shear layer mixing region

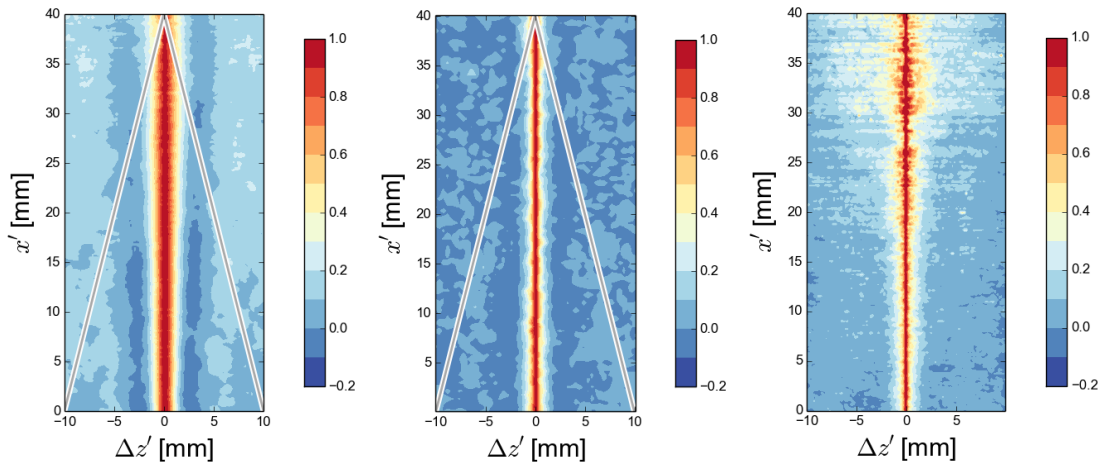

(a) Solid serration (b) Slitted serration (c) Straight trailing edge

Figure 11: Spanwise cross-correlation maps for u', where $\alpha = 6°$, $\varphi = 0°$, and $U_\infty = 20$ m/s, over the pressure side, and relative to $z'_0 = 0$ mm.

behind the trailing edge, but which cannot be confirmed without performing solely with the measurements here performed. This effect is not seen in the serrated cases, but performing measurements further downstream could unravel the presence of such a trend, and hypothetically show some periodicity in it correlated to the trailing edge shape.

The solid serration also exhibits a streamwise pattern of close to zero cross-correlation at around $z' = \pm 2.5$ mm before the coefficient jumps back to values of around 0.2 ± 0.1, reaching slightly higher values in the empty regions between adjacent serrations. The slitted serration instead shows very small correlation coefficients in most of the plane, regardless of x' or z' location.

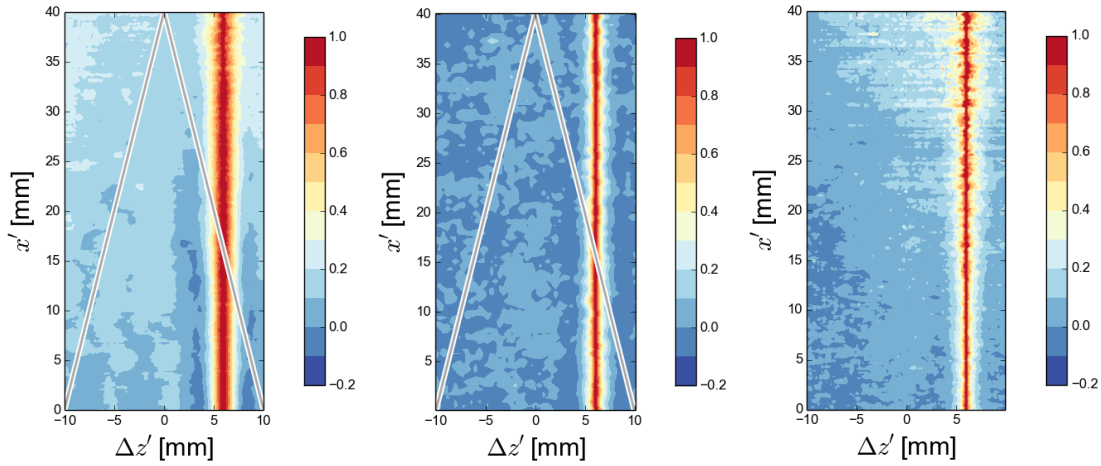

(a) Solid serration (b) Slitted serration (c) Straight trailing edge

Figure 12: Spanwise cross-correlation maps for u', where $\alpha = 6°$, $\varphi = 0°$, and $U_\infty = 20$ m/s, over the pressure side, and relative to $z_0 = 6.6$ mm.

When taking the cross-correlation coefficient in respect to $z'_0 = 6.6$ mm, as in figure 12, similar

patterns emerge as for $z_0' = 0$ mm, with the slitted serrations showing the smallest values over the whole plane. The straight trailing edge also shows the larger coefficient values downstream as seen in figure 11c, but that is natural to expect as a change in the spanwise position of z_0 should not be expected to cause any difference in results, given the lack of spanwise geometric variation of this case.

The solid serration results of figure 12a show again the spanwise pattern near the z_0' area of close to zero values, as seen in figure 11a. Nevertheless, in this case the pattern is markedly disrupted by the serration trailing edge and the pattern shows a slanted behavior, even reaching higher values downstream where the flow is deep in the region between adjacent serrations, but no longer in a symmetric form.

These results seem to suggest that the solid serration design has a clear effect on the flow turbulence properties, as it also had been shown above to have on the time averaged flow properties. The benefits of the slitted serrations are again replicated in the turbulence analysis given through these measurements, indicating that they have a minimal effect on the flow. The comparison between the serrated cases and the straight trailing edge case also offers a sample of the overall impact that a variable trailing edge has on the flow, and it points to a potential region of interest further behind the serrations where the flow is clear of the solid—or permeable—blockage that they induce.

4. Simulation results

In order to establish the success of the simulation campaign, a baseline case has been chosen based on the NACA 0018 airfoil for an angle of attack of $\alpha = 6^\circ$ and $\varphi = 0^\circ$ serration flap angle. A vector plane is extracted from the numerical model at roughly the same location as that which was used in the experimental campaign, relative to the serration pressure side surface, $\sim 0.1\delta$.

Nevertheless, as can be seen in figure 13, the computational results are satisfactorily close to the experimental measurements. Here half a serration width is presented, with the serration midline on the right axis at $z' = 0$. The same pattern and magnitudes are clearly observed for this flow component in regions over the serration trailing edge. There exist nevertheless interesting differences between the two, most notably in the serration midline region, where the computational results don't agree with a zero magnitude for this component, which on the

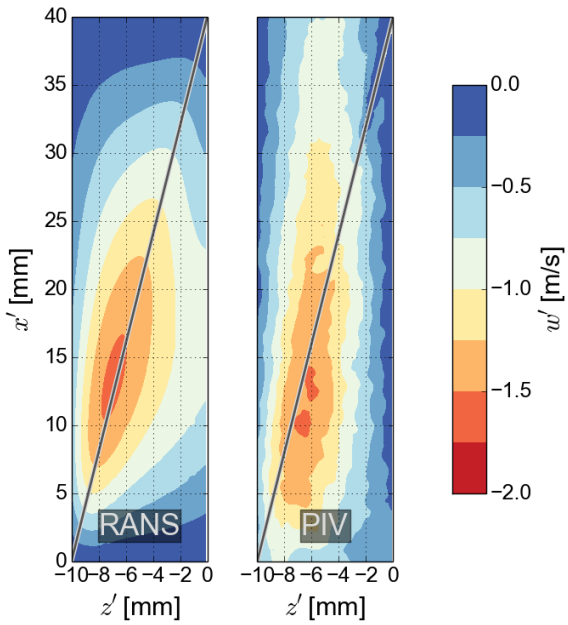

Figure 13: Comparison between computational and experimentally obtained results for the NACA 0018 case at 6° angle of attack and 0° flap angle. Only half a serration width is shown.

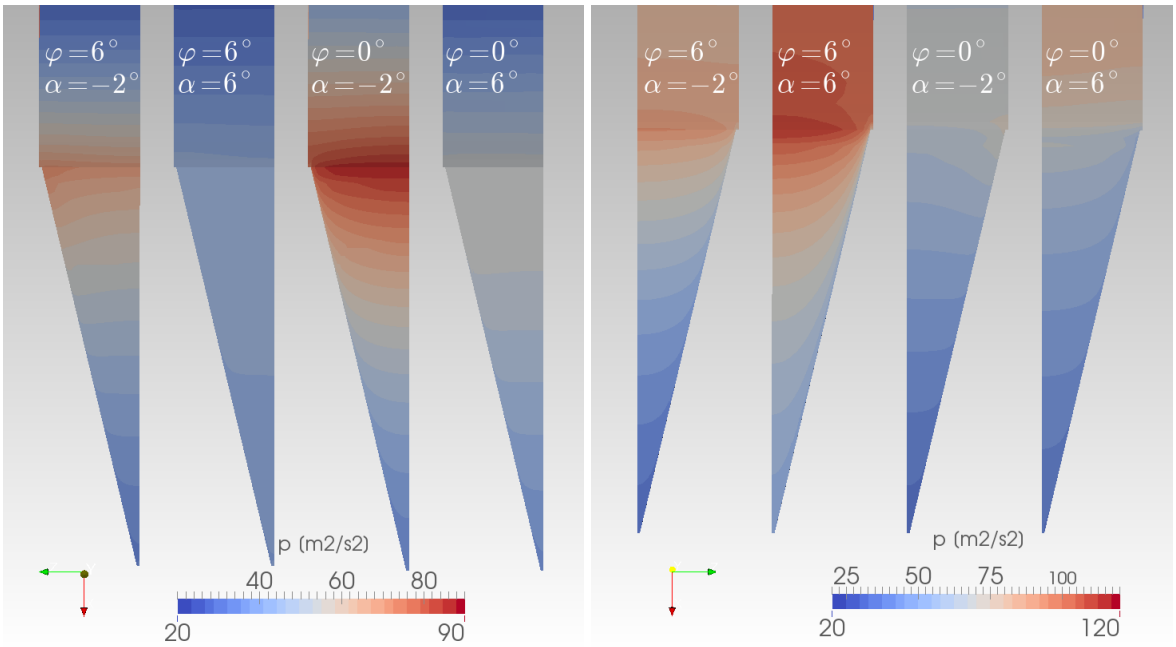

(a) Upper airfoil surface

(b) Lower airfoil surface

Figure 14: Surface pressures for the DU96 case as solved by RANS.

contrary should be expected from the presumed axisymmetry along this line, and which is confirmed in the experimental results.

Additionally, the results upstream, close to the serration root, also appear to disagree, the computational results showing zero magnitude while in the experimental case this region seems to follow the flow deflection trend seen further downstream along the trailing edge. Perhaps more critically, there is a notable disagreement downstream of the serration, where the PIV measurements show a stronger spanwise flow component that is absent in the RANS results. This indicates that there will likely be a general disagreement towards the effects of the serration on the flow in the wake, and differences in for example spanwise vorticity can be expected as consequence.

Since both computational campaigns, pertaining to the NACA 0018 and DU96 airfoil cases, follow the same meshing philosophy and solver settings, it will be further assumed that the fidelity of the results, as here established for the NACA 0018 campaign, will also be applicable for the DU96 cases discussed below.

In keeping focus on serration incidence effects on flow, the DU96 case is of interest because it is a cambered airfoil, in contrast to the NACA 0018. This means that the design of the serration, assuming the objective of creating the least amount possible of disturbance in the flow for a given angle of attack, is not as straightforward. While for a symmetric airfoil one can expect that at zero lift there would be no differences in pressure between its upper and lower surfaces, this is not the fact for a cambered airfoil, which results in a more complex definition of the serration neutral flap angle. Since the state-of-the-art wind turbine blade design calls for the use of cambered profile sections, finding a method to correctly define the neutral flap angle is the more critical for succeeding at this design application.

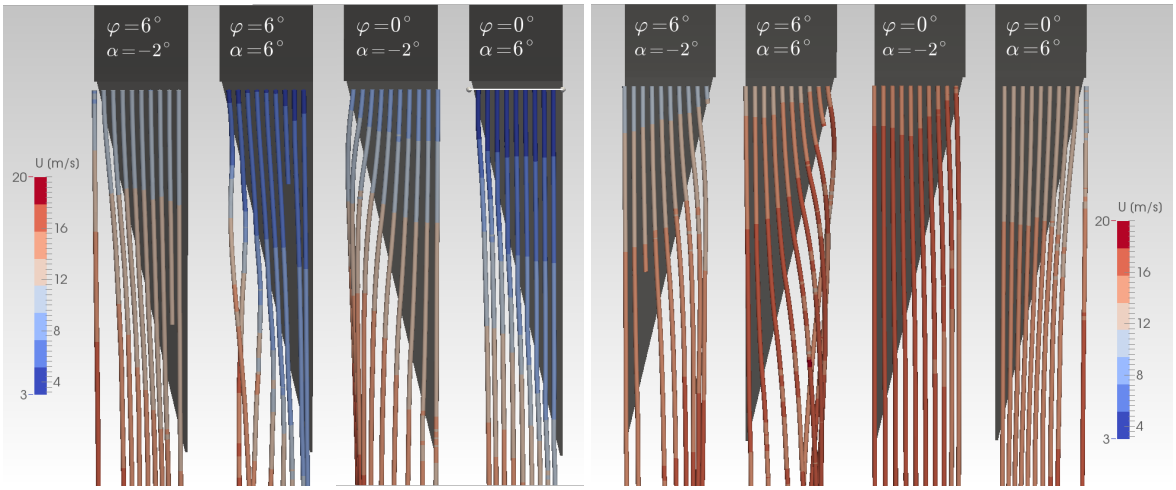

(a) Upper airfoil surface

(b) Lower airfoil surface

Figure 15: Streamlines for the DU96 case as solved by RANS, emitted at $\sim 0.1\delta$ above the airfoil trailing edge.

Using 2D RANS in preparation to the wind tunnel experiment and the more detailed 3D RANS simulations, it was established that the serration neutral flap angle for the 6° airfoil design angle of attack is $\varphi = 0^\circ$ measured against the airfoil chordline. Indeed, when comparing the surface pressure results on figures 14a and 14b, the $\varphi = 0^\circ, \alpha = 6^\circ$ case, shows the lowest pressure gradients when taking the pressure and suction sides into consideration, confirming that the choice of $\varphi = 0^\circ$ is at least a good approximation to what the neutral flap angle should be.

Likewise, the streamline results of figures 15a and 15b also show minimal disturbance for the $\varphi = 0^\circ, \alpha = 6^\circ$ case. The flow in three of the cases exhibits the slight inward curving seen on the suction side streamlines, as suggested by the experimental measurements on the NACA 0018 discussed above. This is so except for the $\varphi = 0^\circ, \alpha = -2^\circ$ case, which has the serration incident to the flow on the upper side of the airfoil instead of the lower, thus reversing the pressure and suction sides. It is also the case which registers the largest surface pressure values on its suction side. The angle of attack in this case causes the flow to seep through the teeth from the upper to the lower side, opposite from that seen in the other cases.

The $\varphi = 6^\circ, \alpha = 6^\circ$ case exhibits the largest flow disturbance as would be expected, being the case with the largest degree of incidence in relation to the others shown. Its considerable effect on the flow, especially on the lower airfoil side is evident by the strong flow deflection above the serration trailing edge, and the streamwise vortex formation, which can be seen on the extreme right side of the field of view, is also visible in the upper airfoil surface visualization of figure 15a.

The fact that the $\varphi = 0^\circ, \alpha = 6^\circ$ case causes the least disturbance on the flow suggests that this is at least a good design approximation for the serration flap angle. Despite the large angle of attack change between $\alpha = 6^\circ$ and -2°, the $\varphi = 0^\circ, \alpha = -2^\circ$ case shows less disturbance than the cases for which $\varphi = 6^\circ$. This reinforces the argued importance of the flap angle as being more influential than angle of attack on flow disturbance due to incidence.

5. Conclusions

A study of trailing edge serrations investigating the impact that incidence has on flow properties, such as time averaged flow streamline behavior and turbulence statistics, has been presented. A NACA 0018 airfoil and a DU96-W-180 airfoil have been used as test beds, and solid and permeable serration designs have been applied, using a combination of experimental and numerical methods for studying the flow, given different degrees of incidence. While the latter were shown to compare well to the experimental measurements, it would be wise to invest further time on improving accuracy at the wake in order to more reliably capture the complex flow behavior in this region.

Overall findings indicate that the flap angle of the serrations is of larger importance than the incidence prescribed through a change in angle of attack. When designing trailing edge serrations for their implementation on wind turbine blades, the relatively low impact of serration incidence found on flow behavior through changes in angle of attack is beneficial. This is due to the fact that, under normal operating conditions, changes in angle of attack are more commonly induced by factors that are relatively hard to mitigate for current technologies. These include wind gusts, misaligned yaw, and wind shear across the rotor plane. Instead, flap angle deviations from the optimal setting can be minimized through careful design of the device, mindful installation, and keeping within correctly defined manufacturing tolerances.

Furthermore, the findings also show that the use of permeable serration designs, such as the tested slitted serrations, helps avoiding the effects on flow of incidence seen for the solid serration design. The presented measurements are proof of the notable differences seen in flow sensitivity to the two different serration designs, and potentially offer promising insight to better understanding the relationship between flow topology and noise reduction efficiency.

Analysis of the turbulent properties of the flow close to the serration surface and in the wake of straight trailing edge also reflect the differences seen between the solid and slitted serrations, showing the latter to allow the flow to retain similar properties to that of the straight trailing edge, despite the applied degree of incidence.

Supported by the fact that these slitted serrations have been measured acoustically by Gruber, Joseph, and Azarpeyvand, 2013 to have better noise reduction performance than the solid serration design, the differences herein presented regarding their effect on the flow can help lead further research towards better identifying those flow parameters that are essential to ensuring effective noise mitigation, ideally resulting in new and innovative designs for devices that are optimized for the conditions encountered in wind turbine blade applications.

References

Arce, C et al. (2015). “Flow Field Around a Serrated Trailing Edge at Incidence”. en. In: *33rd Wind Energy Symposium*. Kissimmee, Florida: American Institute of Aeronautics and Astronautics. ISBN: 978-1-62410-344-5. DOI: 10.2514/6.2015-0991.

Brooks, TF, DS Pope, and MA Marcolini (1989). “Airfoil self-noise and prediction”. In: *National Aeronautics and Space Administration Reference Publication Number 1218*.

Chong, TP, Phillip Joseph, and Mathieu Gruber (2012). “On the airfoil self-noise reduction by trailing edge serrations of non-insertion type”. In: *18th AIAA/CEAS Aeroacoustics Conference*. June, pp. 4–6. DOI: 10.2514/6.2012-2185.

Dassen, T et al. (1996). *Results of a wind tunnel study on the reduction of airfoil self-noise by the application of serrated blade trailing edges*. Tech. rep. National Aerospace Laboratory, NLR.

Gruber, M, M Azarpeyvand, and P Joseph (2010). “Airfoil trailing edge noise reduction by the introduction of sawtooth and slitted trailing edge geometries”. In: *Proceedings of 20th International Congress on Acoustics, ICA* 10.

Gruber, M, P Joseph, and M Azarpeyvand (2013). “An experimental investigation of novel trailing edge geometries on airfoil trailing edge noise reduction”. In: *19th AIAA/CEAS Aeroacoustics Conference*. Reston, Virginia: American Institute of Aeronautics and Astronautics. ISBN: 978-1-62410-213-4. DOI: 10.2514/6.2013-2011.

Howe, MS (1991). “Aerodynamic noise of a serrated trailing edge”. In: *Journal of Fluids and Structures* 5.1, pp. 33–45. DOI: 10.1016/0889-9746(91)80010-B.

Moreau, DJ (2012). “Experimental investigation of flat plate self-noise reduction using trailing edge serrations”. In: *Congress of the International Council of the Aeronautical Sciences*. Brisbane, pp. 1–10.

Moreau, DJ, LA Brooks, and CJ Doolan (2011). “Flat plate self-noise reduction at low-to-moderate Reynolds number with trailing edge serrations”. In: *Proceedings of the Annual Conference on the Australian Acoustical Society*.

Oerlemans, S, P Sijtsma, and B Méndez López (2007). “Location and quantification of noise sources on a wind turbine”. In: *Journal of sound and vibration* 299.4, pp. 869–883. DOI: 10.1016/j.jsv.2006.07.032.

Oerlemans, S et al. (2009). “Reduction of wind turbine noise using optimized airfoils and trailing-edge serrations”. In: *AIAA Journal* 47.6, pp. 1470–1481. ISSN: 0001-1452. DOI: 10.2514/1.38888.

Willmarth, W. W. and S. S. Lu (2006). “Structure of the Reynolds stress near the wall”. English. In: *Journal of Fluid Mechanics* 55.01, p. 65. ISSN: 0022-1120. DOI: 10.1017/S002211207200165X.